Journal of Inorganic Biochemistry 279 (2026) 113271

Contents lists available at ScienceDirect

Journal of Inorganic Biochemistry

journal homepage: www.elsevier.com/locate/jinorgbio

Cyclodextrin–siderophore conjugates as a Trojan horse strategy for bacterial targeting

Chiara Ragusa [a,1], Roberta Panebianco [a,1], Vincenzo Paratore [a], Guglielmo Guido Condorelli [a], Kaveh Eskandari [b], Douglas Robinson [b], Fraser J. Scott [b], Rosanna Inturri [c], Maria Serena Rossitto [c], Valentina Giglio [d], Graziella Vecchio [a,*]

[a] Dipartimento di Scienze Chimiche, Università degli Studi di Catania, Viale A. Doria 6, 95125 Catania, Italy
[b] Department of Pure and Applied Chemistry, University of Strathclyde, Glasgow G1 1XL, United Kingdom
[c] Fidia Farmaceutici S.p.A., Local Noto Unit, Contrada Pizzuta s.n.c., 96017 Noto, Italy
[d] Institute of Biomolecular Chemistry CNR-ICB, Via Paolo Gaifami 18, Catania, Italy

ARTICLE INFO

Keywords:
Antibiotic
Cyclodextrin
Deferoxamine
Doxocycline
Iron

ABSTRACT

The rise of antibiotic resistance necessitates the development of innovative strategies to enhance the effectiveness of existing treatments. One promising approach leverages bacterial iron acquisition systems through siderophore-based drug delivery to increase intracellular drug concentrations, a Trojan horse strategy. We synthesized new cyclodextrin conjugates with siderophores, such as deferoxamine and gallic acid, to exploit the cyclodextrin drug inclusion capability within the Trojan horse strategy. These novel derivatives were investigated as doxycycline carriers in the bacteria *Escherichia coli* and *Staphylococcus aureus*. Notably, the cyclodextrin deferoxamine derivative significantly enhanced the doxycycline efficacy by a 4-fold improvement of its minimal inhibitory concentration against *Escherichia coli*.

1. Introduction

Antibiotic resistance poses an increasing threat to public health. However, developing new drugs is challenging due to the high costs, long time required for clinical trials and high failure rates [1–3]. Consequently, research has focused on innovative strategies to improve the effectiveness of current antimicrobials [2,4–6].

Targeted drug delivery has proven effective in combating bacterial infections, offering some hope in overcoming bacterial resistance mediated by cell wall permeability [7].

One of the most promising research areas is the exploitation of bacterial iron acquisition systems. This Trojan horse approach, based on hijacking the mechanism of iron uptake via siderophore receptors, can improve intracellular concentrations of both small and macromolecular therapeutics [7].

Over the last few decades, several siderophore-antibiotic conjugates (SACs) have been designed using different linkers and siderophore types [8]. In some cases, synthetic siderophores have been conjugated. Some molecules have undergone drug discovery and entered preclinical and clinical trials. A successful example of an SAC is cefiderocol (brand name FeTroja, Fig. 1), which received approval from the Food and Drug Administration (FDA) in 2019 for the treatment of urinary tract infections and in 2020 for nosocomial and ventilator-associated bacterial pneumonia [9]. In addition, it was submitted as part of a phase II clinical trial to assess safety, tolerability, and pharmacokinetics in pediatric hospitalized patients with suspected or confirmed aerobic Gram-negative bacterial infection [10]. Cefiderocol shows an innovative mechanism of cellular entry via siderophore transporters and overcoming resistance to β-lactamases. It demonstrated exceptional *in vitro* efficacy against a broad spectrum of clinically significant Gram-negative pathogens, including multidrug-resistant strains [11]. Cefiderocol contains catechol units, which can form an iron (III) complex recognized by iron transporter channels, enhancing its uptake into bacteria [12].

Among the most commonly used natural siderophores, catechols

Abbreviation: CD, cyclodextrin; DFO, deferoxamine B; DX, doxycycline; ID-MHB2, iron-depleted Mueller-Hinton broth; MHB2, Mueller Hinton broth; MIC, Minimum Inhibitory Concentration; GA, gallic acid; SAC, siderophore-antibiotic conjugate; TLC, thin-layer chromatography.

* Corresponding author.
E-mail address: gr.vecchio@unict.it (G. Vecchio).
[1] These authors contributed equally to this work.

https://doi.org/10.1016/j.jinorgbio.2026.113271
Received 28 November 2025; Received in revised form 9 February 2026; Accepted 16 February 2026
Available online 19 February 2026

[3,13], deferoxamine B [14,15] and enterobactin [16] have been conjugated to antibiotics [3,8,13,15,17–19].

Deferoxamine B (DFO) is a naturally occurring tris-hydroxamic acid siderophore widely produced by different species belonging to the genus *Streptomyces* such as *S. pilosus*, *S. coelicolor*, and *S. griseus*, thanks to the desABCD gene cluster [20]. In the presence of ferric ions, DFO forms a six-coordinate iron complex. It is also used to treat iron overload conditions, such as β-thalassemia and hemochromatosis, as well as aluminum poisoning [21]. Moreover, DFO has been studied for its neuroprotective effects in diseases such as Alzheimer's disease, where iron accumulation may contribute to neurodegeneration [22].

DFO can also form complexes with gallium (III). A recent study has demonstrated that gallium complexes of polymeric DFO conjugates can be taken up by bacteria through an iron uptake system and enhance the antibacterial activity of vancomycin *in vitro* and *in vivo* against Gram-negative bacteria, such as *P. aeruginosa* [23,24].

Gallic acid (3,4,5-trihydroxybenzoic acid, GA) is a biological polyphenol that contains the key catecholate moiety responsible for iron (III) chelation in natural catecholic siderophores [8,25]. GA has been demonstrated to inhibit bacterial biofilm formation [26]. GA has many biological activities [25] and has been conjugated to biomolecules, conferring antibacterial and anticancer properties [27,28].

Based on the interest in SACs, we explored the Trojan horse approach, exploiting non-covalent systems based on cyclodextrin chemistry. Non-covalent drug delivery systems offer many advantages compared to the covalent approach, such as flexibility, reversibility, and reduced toxicity [29,30].

Cyclodextrins (CDs) are cyclic oligosaccharides of glucose units linked by α-1,4-glycosidic bonds. Their truncated cone shape with an inner cavity confers them the ability to form inclusion complexes with a variety of molecules [31].

Due to these properties, CDs are widely used in pharmaceutical applications to enhance the solubility, stability, organoleptic properties, and bioavailability of drugs [32,33]. Notably, CDs and their derivatives exhibit low toxicity and immunogenicity and have been demonstrated to be particularly efficient as drug delivery systems, improving drug therapeutic effects and safety profiles [32]. Currently, more than fifty CD-based formulations are available on the market for a wide range of therapeutic activities, including antibacterial agents such as cefotiam, cefditoren, pivoxil, chloramphenicol, and norfloxacin [34].

In this study, we conjugated DFO or GA with β-CD to form CDDFO and CDGA, respectively (Fig. 1). CDs can act as a binding site for the drug. DFO or GA units incorporated in the CD structure can form complexes with Fe^{3+}, subsequently characterized by UV–Vis spectroscopy and ESI-MS spectrometry. Iron complexes of CDGA and CDDFO may be internalized in bacteria through specific iron uptake channels.

New siderophore CD conjugates were also tested in two reference bacterial strains as novel doxycycline (DX) carriers (Fig. 1). The

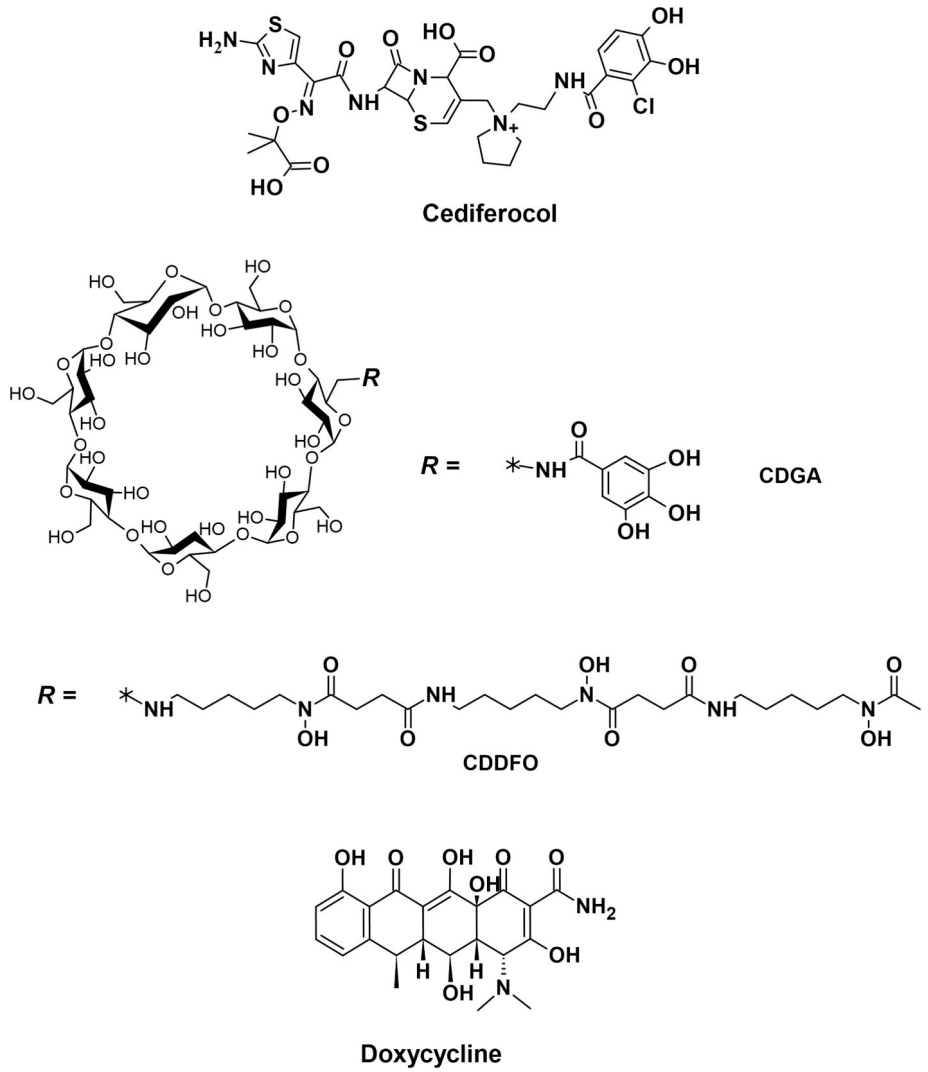

Fig. 1. Cyclodextrin functionalized with gallic acid (CDGA) and deferoxamine (CDDFO), doxycycline (DX) and cefideracol.

Minimum Inhibitory Concentration (MIC) of DX alone and in the presence of siderophore conjugates CDGA and CDDFO was determined against *Escherichia coli*, an example Gram-negative bacterium, and *Staphylococcus aureus*, an example Gram-positive bacterium. *E coli* and *S. aureus* can utilize a variety of exogenous siderophores, including DFO [35,36].

DX is a broad-spectrum tetracycline antibiotic used to control and treat skin, periodontal, and sexually transmitted infections, malaria, and Lyme disease; it is also effective in treating outbreaks such as cholera, mycoplasma, tularemia, typhoid fever, and rickettsiosis [37].

The inclusion complex of DX into β-CD and hydroxypropyl-CD has been extensively investigated [38–40]. It has been reported that the DX-β-CD formulation may enhance photostability and improve drug performance [31,32]. In some countries, pharmaceutical formulations containing DX as inclusion complexes with β-CDs are marketed. These formulations (brand name Doxydan, Doxid Plus, Doxirite, Cyclidox), are used clinically as broad-spectrum antibacterial agents.

2. Material and methods

2.1. Chemicals

Commercially available reagents were used directly unless otherwise stated. Mono-6-O-(p-toluenesulfonyl)-β-cyclodextrin (CDTos) and 6-monoamino-6-monodeoxy-β-cyclodextrin ($CDNH_2$) were purchased from Cyclodextrin-Shop. 1-ethyl-3-(3-dimethylaminopropyl)carbodiimide (EDC), DFO mesylate, triethylamine (TEA) and anhydrous dimethylformamide (DMF) were purchased from Sigma-Aldrich. Gallic acid, 1-Hydroxybenzotriazole (HOBt), and doxycycline hyclate (DX) were purchased from Tokyo Chemical Industry (TCI).

TLC (thin-layer chromatography) was performed on silica gel plates (Merck 60-F254). Carbohydrate derivatives were detected on TLC with the anisaldehyde test and UV light.

2.2. Synthesis of β-cyclodextrin 6-functionalized with gallic acid (CDGA)

EDC (24.5 mg, 0.128 mmol) and HOBt (17.3 mg, 0.128 mmol) were added to a DMF solution (2 mL) of GA (14.5 mg, 0.085 mmol). After 10 min, $CDNH_2$ (100 mg, 0.085 mmol) and TEA (6 μL, 0.04 mmol) were added. The reaction mixture was stirred for 48 h at room temperature under nitrogen. The solvent was evaporated and the crude solid was washed with acetone to remove the unreacted GA. The product was isolated by flash chromatography using an RP C-18 Aq. column and a linear gradient of water/methanol (0 → 100%) as the eluent. Yield 40%. Purity >97% (HPLC, reverse-phase C18 column, eluent: linear gradient H_2O → CH_3OH (20%).

TLC: Rf = 0.53 (PrOH/AcOEt/H_2O/NH_3, 3:3:3:4).

ESI-HRMS: $m/z = [L + H]^+$ calcd for $C_{49}H_{76}NO_{38}$ 1286.4040, found 1286.3988, $[L + Na]^+$ calcd for $C_{49}H_{75}NO_{38}$ Na 1308.3860, found 1308.3788.

^{1}H NMR (500 MHz, D_2O) δ (ppm): 6.85 (s, 2H, H of GA), 5.02 (d, 1H, J = 3.82 Hz, H-1B of βCD), 5.00–4.97 (m, 3H, H-1 of CD), 4.95 (d, 1H, J = 3.75 Hz, H-1F of CD), 4.93 (d, 1H, J = 3.72, H-1A of CD), 4.90 (d, 1H, H-1G, J = 3.75 Hz, of CD), 4.03 (d, 1H, H-6A of CD), 3.95–3.73 (m, 15H, H-3,-5,-6 of CD), 3.69–3.44 (m, 17H, H-2, H-4, H-6B, H-6G of CD), 3.35 (t, 1H, H_4A of CD), 3.22–3.16 (m, 2H, H-6G and H-6A of CD).

^{13}C NMR (125 MHz, D_2O) δ (ppm): 169.2 (CONH), 144.9 (C-3, -5), 136.8 (C-4), 121.0 (C-1), 107.3 (C-2,-6 of GA), 102.1–101.0 (C-1 of CD), 83.3 (C-4A), 81.1 (C-4), 72.9 (C-5), 71.8 (C-3), 71.2 (C-2), 60.3 (C-6), 59.7 (C-6Y), 59.1 (C-6X), 40.8 (C-6A)

2.3. Synthesis of β-cyclodextrin 6-functionalized with deferoxamine B (CDDFO)

CDTos (168.0 mg, 0.143 mmol) was added to DFO (300.0 mg, 0.430 mmol) in DMF (4 mL). The reaction mixture was stirred at 70 °C for 36 h under nitrogen.

The mixture was purified by CM-Sephadex C-25 column (NH_4^+ form) using a linear gradient H_2O-NH_4HCO_3 (0 → 0.2 M) as the eluent. Yield 30%. Purity >96% (HPLC, reverse-phase C18 column, eluent: linear gradient H_2O → CH_3OH (10%).

TLC: Rf = 0.61 (PrOH/NH_3/H_2O, 5:2:3).

ESI-HRMS: $m/z = [L + H]^+$ calcd for $C_{76}H_{117}N_6O_{42}$ 1677.7198, found 1677.7083; $[L + 2H]^{2+}$ calcd for $C_{76}H_{118}N_6O_{42}$ 839.3636, found 839.3586; $[L + H + Na]^{2+}$ calcd for $C_{76}H_{117}N_6O_{42}Na$, 850.3545, found 850.3475, $[L + H + K]^{2+}$ calcd for $C_{76}H_{117}N_6O_{42}K$ 858.3411, found 858.3386.

^{1}H NMR (500 MHz, D_2O) δ (ppm): 5.01–4.94 (m, 7H, H-1 of CD), 4.0 (m, 1H, H-5A of CD), 3.87–3.75 (m, 25H, H-3,-5,-6 of CD), 3.75–3.40 (m, 21H, H-2,-4,-6A of CD and He, Hw, Hn of DFO), 3.22 (m, H, H-6A of CD), 3.07 (m, 4H, Hh, Hq of DFO), 2.97 (m, 2H, Ha of DFO), 2.70 (m, 4H, Hf, Ho of DFO), 2.57 (m, Hf, Ho of Z isomer of DFO), (m, 2.41 (m, 4H, Hg, Hp of DFO), 2.04 (s, 3H, CH_3 of DFO), 2.01 (s, 3H, CH_3 of Z isomer of DFO), 1.63–1.4 (m, 8H, Hd, Hm, Ht, Hb of DFO), 1.42 (m, 4H, Hi, Hr of DFO), 1.29–1.15 (m, 6H, Hc, He, Hs of DFO).

^{13}C NMR (125 MHz, D_2O) δ (ppm): 174.6 (CONH DFO), 173.6 (CONOH DFO), 102.2 (C-1 CD), 83.4 (C-4A CD), 81.1 (C-4 CD), 73.1 (C-5 CD), 72.0 (C-2 CD), (67.3 (C-5A CD), 60.2 (C-6 CD), 52.5–46.1 (Ca, Cn, Cw, Cl DFO), 41.5 (C-6A of CD), 39.2 (Ch, Cq DFO), 30.2 (Cg, Cp DFO), 28.1–27.7 (Ci, Cr, Ct, Cq, Ch DFO), 27.5 (Cf, Co DFO), 27.0–24.1 (Cd, Cm, Ct, Cb DFO), 22.9 (Cc, Cs, Cl DFO), 19.2 (CH_3 DFO).

2.4. NMR spectroscopy

^{1}H and ^{13}C NMR spectra were recorded at 25 °C with a Varian UNITY PLUS-500 spectrometer at 499.9 and 125.7 MHz, respectively, using standard pulse programs from the Varian library. Two-dimensional experiments (COSY, TOCSY, gHSQC, gHMBC, ROESY) were acquired using 1 K data points, with 256 increments and a relaxation delay of 1.2 s. The glucose units in CD derivatives are labeled A–G clockwise, starting from the modified ring (denoted as A) and viewed from the upper rim.

2.5. ESI-HR mass spectrometry

High-resolution mass spectra were acquired using an Orbitrap Exploris™ Oe120 (Thermo Fisher) in positive electrospray ionization (ESI+) mode. Freshly prepared aqueous solutions of the CD conjugates were injected at a concentration of 10 μM. For the Fe^{3+} complexes, solutions were prepared by mixing a ligand solution with an $FeCl_3$ solution, and these Fe complexes were diluted to 10 μM in water immediately before mass measurements. Sample solutions were injected into the ion source at a flow rate of 30 μL/min, with nitrogen as the desolvation gas. The electrospray capillary voltage was optimized to 2.5 kV to maintain adequate sensitivity and minimize in-source fragmentation. The resolution obtained ranged from 45,000 to 70,000 FMHM. Mass spectra were processed with Xcalibur software (version 3.0). Each species is indicated by the m/z value of the most intense peak of its isotopic cluster. For a more accurate structural assignment, the relative intensity of the peaks in each cluster was compared with that of the peaks in the corresponding simulated model.

2.6. UV–Vis and circular dichroism spectroscopy

UV–Vis spectra were recorded with a Cary 3500 UV/Vis spectrophotometer equipped with a Peltier temperature control module. Circular dichroism spectra were recorded with a JASCO model *J*-1500 spectropolarimeter at 25°C.

Stock solutions of CDGA and CDDFO were prepared in Milli-Q water. $FeCl_3$ solutions were freshly prepared in 2 mM HCl. Complexes were prepared by mixing Fe^{3+} with the corresponding ligand (L) and diluted in 100 mM phosphate buffer at pH 7.4.

The iron(III) titration of CDGA was performed by adding $FeCl_3$

solution to the CDGA solution.

2.7. Antibacterial activity

The minimum inhibitory concentration (MIC) was determined using the microdilution method according to the CLSI (Clinical & Laboratory Standards Institute) guidelines M100-S23 [41].

The two reference strains, *Escherichia coli* ATCC 25922 and *Staphylococcus aureus* ATCC 43300 were used for the assay.

The assay was performed using Mueller Hinton broth 2 (MHB2, Merck). Iron-depleted MHB2 (ID-MHB2) adding 10 g of Chelex® 100 resin (Bio-Rad Laboratories, Hercules, CA) to 100 mL of autoclaved MHB2 and the suspension stirred for 6 h at room temperature (23 °C) to remove cations in the medium [42]. The iron-depleted broth was then filtered using a 0.2 μm filter to remove the resin and the pH of the broth adjusted to 7.3 using 0.1 M HCl. The ID-MHB2 was then supplemented with calcium ($CaCl_2 \bullet 2H_2O$), magnesium ($MgSO_4 \bullet 7H_2O$), and zinc ($ZnCl_2$) to final concentrations of 25 μg/mL (range, 20–25 μg/mL), 12.5 μg/mL (range, 10–12.5 μg/mL), and 1 μg/mL (range 0.5–1.0 μg/mL), respectively, and again passed through a 0.2 μm filter. The final concentration of iron in ID-MHB2 prepared using the above method is ≤0.03 μg/mL [43].

The CDGA and CDDFO systems were tested in combination with DX (CDGA-DX and CDDFO-DX) at a CD/DX molar ratio of 5:1. CDGA or CDDFO was dissolved in a sterile fresh medium and DX was added to obtain a 2× stock solution with a DX concentration of 64 μg/mL. The systems were tested in comparison with the standard antibiotics DX and cefiderocol alone, also prepared in fresh medium at a 2× stock concentration of 64 μg/mL.

For each strain, an inoculum was prepared by suspending a colony, previously grown onto Luria-Bertani agar (LBA) (from a stock stored at −80 °C), in 5.0 mL of fresh MHB2 or ID-MHB2 and incubated overnight under aerobic conditions at 37 °C and 140 rpm. Before inoculation, the density of the bacterial suspension was adjusted to achieve a final concentration of about 5.0×10^5 CFU/mL in 100 μL of each well of the 96-well plate. The wells containing the top concentration of test compound were prepared by adding 100 μL of the respective 2× stock solution, for a total volume of 200 μL, before carrying out a 2-fold serial dilution, ranging from 32 to 0.0625 μg/mL. The 96-well plates were then incubated and shaken overnight under aerobic conditions at 37 °C and 140 rpm. MICs were determined in biological triplicate, reporting the modal value. The lowest concentration of systems that completely inhibited bacterial growth was detected by eye after 20 h of incubation, compared to the control growth wells (fresh medium only).

3. Results and discussion

GA and DFO were conjugated with β-CD at the primary rim. CDDFO derivative was synthesized from CDTos through nucleophilic substitution in DMF (Fig. S1). CDGA was synthesized through a condensation reaction starting from $CDNH_2$ and GA, with HOBt and EDC as activating agents (Fig. S2). The NMR spectra of the derivatives were assigned by COSY, TOCSY, HSQC, HMBC and ROESY spectra.

In the ^{1}H NMR spectra of CDDFO (Figs. 2, S3–S6), in addition to the typical signals of CD protons, the protons of DFO resonate between 3.2 and 1.0 and in the H-2, H-4 region of CD. Hs-6A of the functionalized glucose ring were observed upfield shifted compared to free CD, and H-5A resonated at 4.0 ppm downfield shifted in keeping the functionalization of CD with DFO. In the spectra, the small signals at 2.57 and 2.03 ppm of the DFO moiety are due to the Z isomer as reported for free DFO [44].

In the ^{1}H NMR spectra of CDGA (Figs. 3, S7–S12), the aromatic protons of GA resonate at 6.85 ppm; the signals of the H-1 protons of CD are spread over the 5.02–4.90 ppm region, with the H-1A proton at 4.93 ppm. The diastereotopic H-6 protons of the glucose ring functionalized with the amino group resonate at 4.03 and 3.22 ppm. In the spectra, the upfield shift of H-6 protons of B and G rings, adjacent to the A ring, was also evident. The upfield shift is due to the current effect of the aromatic ring faced on the primary rim, as found for similar derivatives [45,46].

CDGA was further studied by ROESY experiments. ROESY spectra of CDGA showed cross peaks between aromatic protons of GA and H-6 protons of B glucose and H-6, H-5 region (Fig. S12), suggesting the proximity of the aromatic ring to the H-6 protons, in keeping with the large upfield shift of the H-6B protons.

3.1. ESI-HR mass spectrometry

The molecular weight of the CD conjugates was confirmed by HR mass spectrometry (Table 1, Figs. S13–S16). The +ESI-HRMS spectrum of CDGA, reported in Fig. S16, shows the peak of the molecular ion [L +

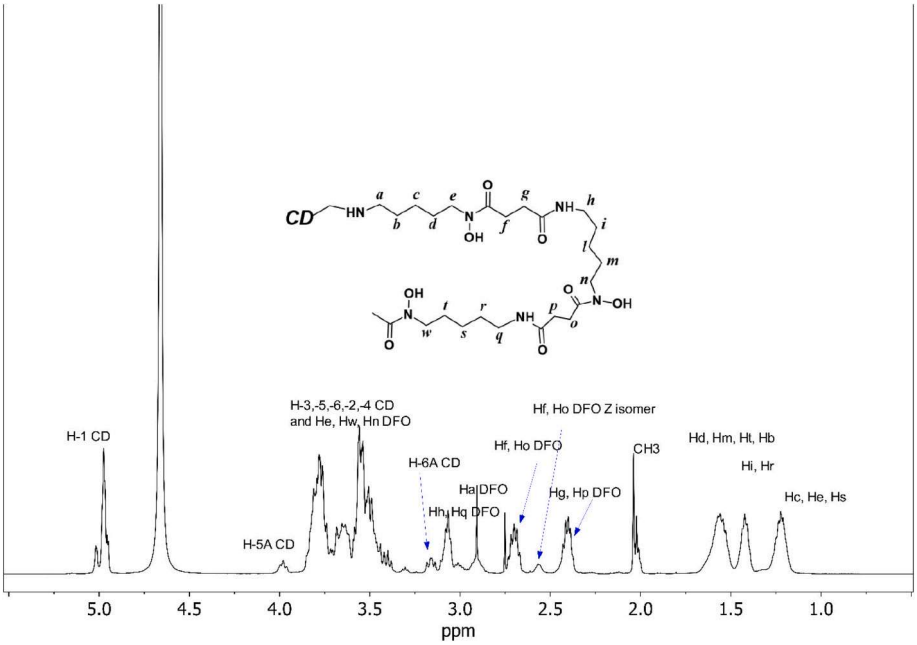

Fig. 2. ^{1}H NMR spectrum of CDDFO (D_2O, 500 MHz).

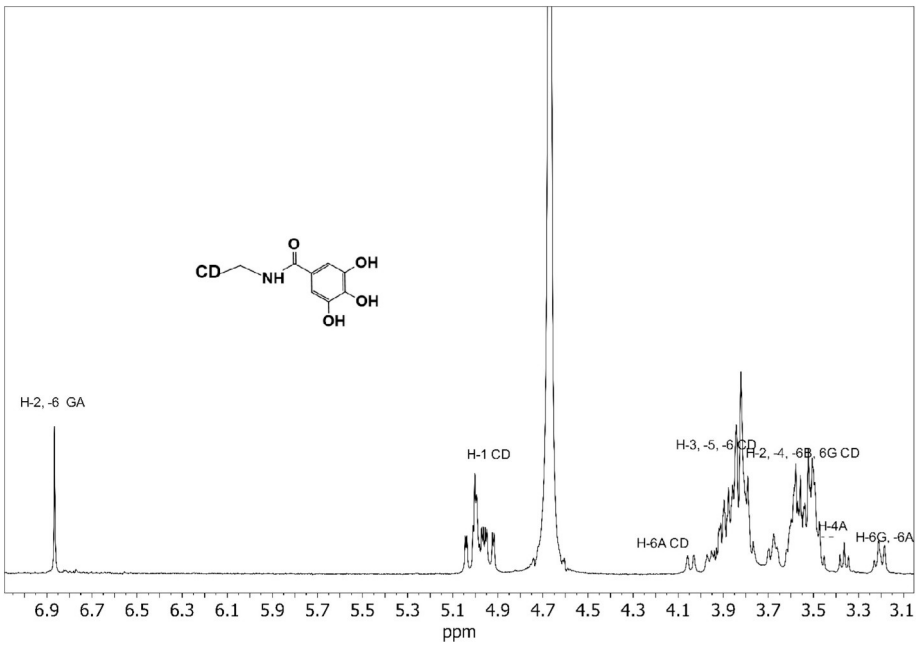

Fig. 3. ^{1}H NMR spectrum of CDGA (D_2O, 500 MHz).

Table 1
Species found and calculated for the CDDFO and CDGA and their Fe^{3+} complexes in ESI-MS.

Compound (L)	Species	Formula	Theoretical (m/z)	Observed (m/z)	Error (ppm)
CDDFO	$[L + H]^+$	$C_{76}H_{117}N_6O_{42}$	1677.7198	1677.7083	6.80
	$[L + 2H]^{2+}$	$C_{76}H_{118}N_6O_{42}$	839.3636	839.3586	5.95
	$[L + H + Na]^{2+}$	$C_{76}H_{117}N_6O_{42}Na$	850.3545	850.3475	8.23
	$[L + H + K]^{2+}$	$C_{76}H_{117}N_6O_{42}K$	858.3411	858.3386	2.91
CDDFO/Fe^{3+}	$[FeL + H]^+$	$C_{76}H_{114}N_6O_{42}Fe$	1730.6313	1730.6232	4.68
	$[FeL + 2H]^{2+}$	$C_{76}H_{115}N_6O_{42}Fe$	865.8193	865.8165	3.23
	$[FeL + H + Na]^{2+}$	$C_{76}H_{114}N_6O_{42}FeNa$	876.8103	876.8056	5.36
	$[FeL + H + K]^{2+}$	$C_{76}H_{114}N_6O_{42}FeK$	884.7972	884.7918	6.10
CDGA	$[L + H]^+$	$C_{49}H_{76}NO_{38}$	1286.4040	1286.3988	4.04
	$[L + Na]^+$	$C_{49}H_{75}NO_{38}Na$	1308.3860	1308.3788	5.50
CDGA/Fe^{3+}	$[FeL]^+$	$C_{49}H_{73}NO_{38}Fe$	1339.3154	1339.3094	4.47
	$[FeL + H]^{2+}$	$C_{49}H_{74}NO_{38}Fe$	670.6653	670.6621	4.77

H]$^+$ at *m/z* 1286.3988 (calcd 1286.4040) and the single-charged sodium adduct $[L + Na]^+$ at *m/z* 1308.3788 (calcd 1308.3860). In the case of deferoxamine conjugate, the +ESI spectrum (Fig. S16) shows the molecular peak ion at 1677.7083 *m/z* (calcd 1677.7198) and double-charged peaks at 839.3586, 850.3475 and 858.3386 m/z corresponding to the $[L + 2H]^{2+}$, $[L + H + Na]^{2+}$ and $[L + H + K]^{2+}$ species respectively. The identity of the synthesized derivatives was further confirmed by comparing the experimental isotope distribution of the molecular ion peak with the theoretical isotope distribution for the two cyclodextrin conjugates (Figs. S15 and S16).

3.2. Circular dichroism spectroscopy

The inclusion complex of DX in the CDs has been widely characterized [38–40]. We used circular dichroism spectroscopy to investigate the interactions between CDDFO and CDGA and the drug DX. In the 220–450 region, CDDFO did not exhibit dichroic bands (Fig. 4), and CDGA only exhibited a lower band at about 220 nm, due to the aromatic side linked to the chiral cavity. UV–Vis spectra were also carried out (Fig. S17). In the circular dichroism spectra of DX (Fig. 4), intense positive dichroic bands at 270 and 296 nm (positive) and a negative band at 327 nm were observed as reported for tetracycline drugs [47]. The circular dichroic spectra of DX depend on the conformation of the ring and are influenced by the solvent polarity [48]. In the presence of

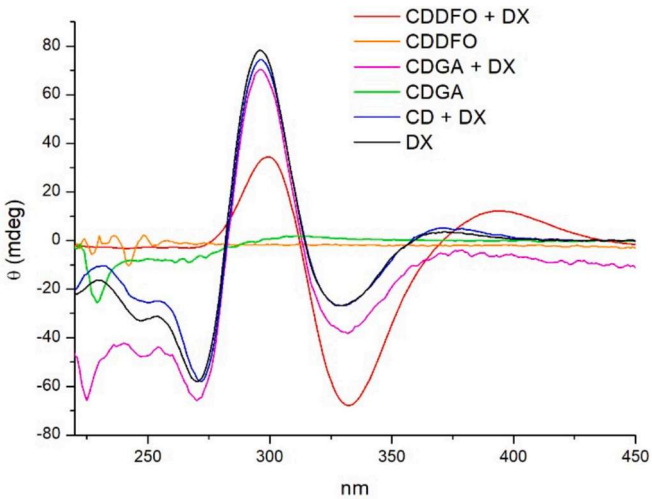

Fig. 4. Circular dichroism spectra of DX (7.8×10^{-4} M) in the presence of CDDFO, CDGA and CD in water at pH 7. Circular dichroism spectra of CDGA and CDDFO are also reported.

CD and its derivatives, the band intensities of circular dichroism spectra

changed, and this can be assigned to a different conformation of the tetracycline ring due to the interaction with the CD cavity. The circular dichroism spectra of CDGA-DX and CD-DX are very similar to the spectra of DX. Particularly, the circular dichroism spectra of CDDFO-DX showed a more intense negative band at 330 nm and a weaker positive band at 299 nm compared to DX. These differences in the circular dichroism spectra of DX with CDDFO can suggest a best interaction between the tetracycline ring and the cyclodextrin cavity of CDDFO compared to CD or CDGA. We can hypothesize that the DFO chain can facilitate DX interaction with the cavity.

3.3. Iron complexes of CDGA and CDDFO

CDDFO and CDGA can form iron (III) complexes, which were investigated through UV–Vis spectroscopy. DFO contains three hydroxamate groups that exhibit a high affinity for Fe^{3+} ions [21,49]. Equilibrium studies of the DFO/Fe^{3+} system confirmed the formation of a 1:1 complex. Within the pH range of 1 to 10, the dominant species is the $[Fe(DFO)]^+$ complex, with the amino group protonated, with a high stability constant (logβ 41.5) [21]. Typically, the functionalization of chelators with CD does not significantly reduce the ability of the ligand moiety to form metal complexes, as reported for similar systems [24,25], and we can hypothesize similar stability constants for Fe^{3+}-CDDFO complexes. In the UV–Vis spectrum of CDDFO, in the presence of Fe^{3+} in M/L 1:1 molar ratio (Fig. S18), the characteristic LMCT (Ligand-to-metal charge transfer) transition at 428 nm typical of the $[Fe(DFO)]^+$ complex [50] was observed, in keeping with the formation of the $[Fe(CDDFO)]^+$ complex.

GA forms highly stable complexes with iron (III) with $logK_1$ 14.73 and log K_2 11.93 [51–53]. The UV–Vis spectra suggested a similar behavior for the CDGA ligand. The UV–Vis spectra of the CDGA/Fe^{3+} at 7.4 showed the formation of the complexes. In the spectra, the peak at 259 nm due to the $\pi \rightarrow \pi^*$ ligand transition is shifted due to the deprotonation of the OH groups in the complex species, as reported for GA [54]. Furthermore, a new band appeared in the visible region at around 538 nm due to a LMCT transition, as reported for iron GA complexes [53] (Fig. 5). The absorbance values changed with the molar ratio up to 2:1 L/M (Fig. S19), suggesting the formation of $[Fe(CDGA)_2]^-$ species at pH 7.4 as found for GA and other catecholates at the same pH value [51–53,55].

The formation of the CDDFO/Fe^{3+} complex was also confirmed by ESI–MS (Table 1), as shown in Fig. S20. The signals corresponding to mono- and diprotonated species, due to the species $[Fe(CDDFO) + H]^+$ and $[Fe(CDDFO) + 2H]^{2+}$, were observed at *m/z* 1730.6232 (calcd 1730.6313) and *m/z* 865.8165 (calcd 865.8193), respectively. In addition, the double-charged peaks at 876.8056 (calcd 876.8103) and *m/z* 884.7918 (calcd 884.7972) were detected in the spectra due to $[Fe(CDDFO) + H + Na]^{2+}$ and $[Fe(CDDFO) + H + K]^{2+}$, respectively.

The formation of $[Fe(CDGA)]^+$ complex with 1:1 stoichiometry was also confirmed by ESI-MS. As shown in the inset of Fig. S21, the signals of molecular ion peak $[Fe(CDGA)]^+$ at 1339.3094 *m/z* (calcd 1339.3154) and its double-charged peak at 670.6621 *m/z* (calcd 670.6653) were detected, while the peak corresponding to the $[L + H]^+$ species was still detectable. However, even by varying the L/M ratio up to 3:1 and recording the spectra in negative-ESI mode, no higher stoichiometry species were detected. Due to the high molecular weight of the FeL_2 and FeL_3 species, their formation could not be confirmed under the working and instrumental conditions used. Table 1 summarizes the experimentally observed and calculated *m/z* values for all ligands and their Fe^{3+} complexes investigated.

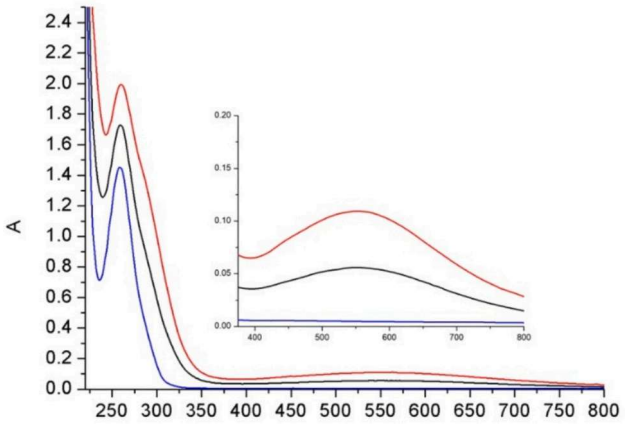

Fig. 5. UV–Vis spectra of CDGA (blue) and CDGA-Fe^{3+} complexes at 2:1 (black) and 1:1 (red) CDGA/Fe^{3+} ratio at pH = 7.4. CDGA is 1.8×10^{-4} M. (For interpretation of the references to colour in this figure legend, the reader is referred to the web version of this article.)

3.4. Antibacterial activity

Staphylococcus aureus ATCC 43300 and *Escherichia coli* ATCC 25922 were used as Gram-positive and Gram-negative bacteria models, respectively. MICs were determined using the microdilution method in Mueller-Hinton Broth 2 (MHB2) or iron-depleted MHB2 (ID-MHB2), at twofold serial dilutions in the 32–0.0625 μg/mL range (Table 2). The CDGA and CDDFO systems were tested alone, and in combination with DX (CDGA-DX and CDDFO-DX) at a 1:5 DX/CD molar ratio and their MICs determined based on the concentration of DX to be able to compare to DX alone. This 5:1 ratio of the cyclodextrin systems to doxycycline was used to promote complexation and ensure efficient loading of the antibiotic onto the carrier. Cefiderocol was used as a functional control to confirm that iron-depleted conditions produced the expected biological response for a siderophore-mediated antibiotic control [42].

The MICs of DX alone were in line with those expected from the literature, with an MIC of 0.125 μg/mL against *E. coli* and 2 μg/mL against *S. aureus*, and no change in MICs in the iron-depleted environment. Both CDGA and CDDFO alone were inactive against both organisms, with MICs >32 μg/mL.

CDGA complexation had no effect on the activity of DX, as CDGA-DX has the MICs as DX. However, complexation with CDDFO exhibited a reproducible 4-fold improvement in the MIC of DX against *E. coli* in the iron-depleted environment, while the other MICs of CDDFO-DX remained the same. This behavior is similar to cefiderocol, which exhibited an 8-fold improvement in MIC against *E. coli*, thought to be due to upregulated components of the iron transporter system [56]. Therefore, the improvement of MIC of CDDFO-DX against *E. coli* in ID-MHB2 is also likely to be due to increased intracellular accumulation via iron transport systems.

We acknowledge that iron chelation by the desferrioxamine moiety

Table 2
MIC values against *S. aureus* ATCC 43300 and *E. coli* ATCC 25922 in MHB2 and ID-MHB2.

Strains/ media	MIC values (μg/mL)					
	DX	CDGA	CDGA-DX (DX + 5 eq. CDGA)	CDDFO	CDDFO-DX (DX + 5 eq. CDDFO)	Cefiderocol
S. aureus ATCC 43300						
MHB2	0.125	>32	0.125	>32	0.125	32
ID-MHB2	0.125	>32	0.125	>32	0.125	16
E. coli ATCC 25922						
MHB2	2	>32	2	>32	2	1
ID-MHB2	2	>32	2	>32	0.5	0.125

could, in principle, contribute to growth inhibition under iron-limited conditions. However, this alone is unlikely to account for the observed phenotype, as doxycycline itself does not display enhanced activity under iron limitation, and CDDFO is inactive in iron-replete media (MHB2), suggesting a conditional, iron-regulated effect rather than nonspecific iron starvation.

4. Conclusion

We synthesized and characterized β-cyclodextrin conjugates with siderophore systems such as deferoxamine and gallic acid. The CD derivatives form iron (III) complexes that can act as carriers for doxycycline in bacteria.

The cyclodextrin functionalized with deferoxamine increased the antibacterial activity of doxycycline in iron-depleted medium, resulting in a 4-fold improvement in the MIC of DX against *Escherichia coli* compared to doxycycline alone. No effect was found for cyclodextrin functionalized with gallic acid.

Although *E. coli* does not synthesize desferrioxamine, it expresses the TonB-dependent FhuA transporter, which mediates uptake of hydroxamate siderophores such as ferrichrome and has been reported to recognise ferrioxamine-type ligands [57–59]. In the present study, we did not perform genetic knockouts or competitive inhibition assays to directly confirm transporter dependence; therefore, while FhuA-mediated uptake of the desferrioxamine–cyclodextrin conjugate is plausible, this remains hypothetical. Future work could employ FhuA-deficient strains or competitive siderophore assays to definitively test whether this pathway contributes to conjugate uptake. Importantly, the observed iron-dependent enhancement of doxycycline activity is consistent with engagement of iron-regulated uptake pathways, even if the precise transporter has not been identified.

We believe the non-covalent approach using cyclodextrin-siderophores offers significant advantages over the covalent approach, including versatility, reversible drug release, enhanced bioavailability, and adaptability to a broad range of antibiotics.

Even if further studies are required to explore the interaction of the cyclodextrin functionalized with deferoxamine with the outer membrane receptors of bacteria and assess its potential as a Trojan horse, our results highlight the effectiveness of cyclodextrin-based siderophores in improving drug efficacy.

CRediT authorship contribution statement

Chiara Ragusa: Writing – review & editing, Writing – original draft, Methodology, Data curation. **Roberta Panebianco:** Writing – review & editing, Writing – original draft, Validation, Investigation, Data curation. **Vincenzo Paratore:** Writing – original draft, Investigation, Data curation. **Guglielmo Guido Condorelli:** Writing – review & editing, Writing – original draft, Methodology, Data curation. **Kaveh Eskandari:** Methodology, Investigation, Data curation. **Douglas Robinson:** Validation, Methodology, Investigation. **Fraser J. Scott:** Writing – review & editing, Writing – original draft, Methodology, Investigation, Data curation, Conceptualization. **Rosanna Inturri:** Writing – review & editing, Methodology, Investigation. **Maria Serena Rossitto:** Investigation, Data curation. **Valentina Giglio:** Writing – review & editing, Writing – original draft, Investigation, Data curation. **Graziella Vecchio:** Writing – review & editing, Writing – original draft, Supervision, Investigation, Funding acquisition.

Declaration of competing interest

The authors declare that they have no competing financial interests or personal relationships that could have influenced the work reported in this manuscript.

Acknowledgments

The authors thank EU funding within the NextGenerationEU-MUR PNRR Extended Partnership initiative on Emerging Infectious Diseases (Project no. PE00000007, INF-ACT) for financial support. DR is funded by Medical Research Scotland (PHD-50237-2020).

Appendix A. Supplementary data

Supplementary data to this article can be found online at https://doi.org/10.1016/j.jinorgbio.2026.113271.

References

[1] B. Plackett, Why big pharma has abandoned antibiotics, Nature 586 (2020) S50–S52, https://doi.org/10.1038/d41586-020-02884-3.
[2] L.J.V. Piddock, R. Malpani, A. Hennessy, Challenges and opportunities with antibiotic discovery and exploratory research, ACS Infect. Dis. 10 (2024) 2445–2447, https://doi.org/10.1021/acsinfecdis.4c00530.
[3] Z.-Y. Miao, J. Lin, W.-M. Chen, Natural sideromycins and siderophore-conjugated natural products as inspiration for novel antimicrobial agents, Eur. J. Med. Chem. 287 (2025) 117333, https://doi.org/10.1016/j.ejmech.2025.117333.
[4] J. Vila, J. Moreno-Morales, C. Ballesté-Delpierre, Current landscape in the discovery of novel antibacterial agents, Clin. Microbiol. Infect. 26 (2020) 596–603, https://doi.org/10.1016/j.cmi.2019.09.015.
[5] D. Heimann, D. Kohnhäuser, A.J. Kohnhäuser, M. Brönstrup, Antibacterials with novel chemical scaffolds in clinical development, Drugs 85 (2025) 293–323, https://doi.org/10.1007/s40265-024-02137-x.
[6] M.S. Butler, W. Vollmer, E.C.A. Goodall, R.J. Capon, I.R. Henderson, M.A. T. Blaskovich, A review of antibacterial candidates with new modes of action, ACS Infect. Dis. 10 (2024) 3440–3474, https://doi.org/10.1021/acsinfecdis.4c00218.
[7] A. Górska, A. Sloderbach, M.P. Marszałł, Siderophore–drug complexes: potential medicinal applications of the 'Trojan horse' strategy, Trends Pharmacol. Sci. 35 (2014) 442–449, https://doi.org/10.1016/j.tips.2014.06.007.
[8] B. Rayner, A.D. Verderosa, V. Ferro, M.A.T. Blaskovich, Siderophore conjugates to combat antibiotic-resistant bacteria, RSC Med. Chem. 14 (2023) 800–822, https://doi.org/10.1039/D2MD00465H.
[9] S. Domingues, T. Lima, M.J. Saavedra, G.J. Da Silva, An overview of Cefiderocol's therapeutic potential and underlying resistance mechanisms, Life (Basel) 13 (2023) 1427, https://doi.org/10.3390/life13071427.
[10] Shionogi, A Single Arm, Open-label Study to Assess the Safety, Tolerability, and Pharmacokinetics of Single and Multiple Doses of Cefiderocol in Hospitalized Paediatric Subjects 3 Months to 18 Years of Age with Suspected or Confirmed Aerobic Gram-Negative Bacterial Infections, clinicaltrials.gov, https://clinicaltrials.gov/study/NCT04335539, 2024 (accessed December 11, 2024).
[11] Y.Y. Syed, Cefiderocol: a review in serious gram-negative bacterial infections, Drugs 81 (2021) 1559–1571, https://doi.org/10.1007/s40265-021-01580-4.
[12] J.Y. Wu, P. Srinivas, J.M. Pogue, Cefiderocol: a novel agent for the management of multidrug-resistant gram-negative organisms, Infect. Dis. Ther. 9 (2020) 17–40, https://doi.org/10.1007/s40121-020-00286-6.
[13] T. Sato, K. Yamawaki, Cefiderocol: discovery, chemistry, and in vivo profiles of a novel siderophore cephalosporin, Clin. Infect. Dis. 69 (2019) S538–S543, https://doi.org/10.1093/cid/ciz826.
[14] C. Ji, M.J. Miller, Siderophore–fluoroquinolone conjugates containing potential reduction-triggered linkers for drug release: synthesis and antibacterial activity, Biometals 28 (2015) 541–551, https://doi.org/10.1007/s10534-015-9830-3.
[15] A. Faucon, J. Renault, I. Josts, J. Couchot, J.-L. Renaud, F. Hoegy, P. Plésiat, H. Tidow, S. Gaillard, G.L.A. Mislin, Synthesis and antibacterial properties under blue LED light of conjugates between the siderophore desferrioxamine B (DFOB) and an iridium(III) complex, Bioorg. Med. Chem. 112 (2024) 117842, https://doi.org/10.1016/j.bmc.2024.117842.
[16] C. Guo, E.M. Nolan, Heavy-metal trojan horse: enterobactin-directed delivery of platinum(IV) prodrugs to *Escherichia coli*, J. Am. Chem. Soc. 144 (2022) 12756–12768, https://doi.org/10.1021/jacs.2c03324.
[17] T. Caradec, E. Anoz-Carbonell, R. Petrov, M. Billamboz, K. Antraygues, F.-X. Cantrelle, E. Boll, D. Beury, D. Hot, H. Drobecq, X. Trivelli, R.C. Hartkoorn, A novel natural siderophore antibiotic conjugate reveals a chemical approach to macromolecule coupling, ACS Cent. Sci. 9 (2023) 2138–2149, https://doi.org/10.1021/acscentsci.3c00965.
[18] S. Fritsch, V. Gasser, C. Peukert, L. Pinkert, L. Kuhn, Q. Perraud, V. Normant, M. Brönstrup, I.J. Schalk, Uptake mechanisms and regulatory responses to MECAM- and DOTAM-based artificial siderophores and their antibiotic conjugates in *Pseudomonas aeruginosa*, ACS Infect. Dis. 8 (2022) 1134–1146, https://doi.org/10.1021/acsinfecdis.2c00049.
[19] V. Lysenko, M.-L. Gao, F.A.C. Sterk, P. Innocenti, C.J. Slingerland, N.I. Martin, Design, synthesis, and antibacterial evaluation of rifampicin–siderophore conjugates, in: ACS Infect. Dis. 11, 2025, pp. 2301–2309, https://doi.org/10.1021/acsinfecdis.5c00311.
[20] D. Eto, K. Watanabe, H. Saeki, K. Oinuma, K. Otani, M. Nobukuni, H. Shiratori-Takano, H. Takano, T. Beppu, K. Ueda, Divergent effects of desferrioxamine on bacterial growth and characteristics, J. Antibiot. 66 (2013) 199–203, https://doi.org/10.1038/ja.2012.111.

[21] D. Bellotti, M. Remelli, Deferoxamine B: a natural, excellent and versatile metal chelator, Molecules 26 (2021) 3255, https://doi.org/10.3390/molecules26113255.
[22] A.C. Farr, M.P. Xiong, Challenges and opportunities of deferoxamine delivery for treatment of Alzheimer's disease, Parkinson's disease, and intracerebral hemorrhage, Mol. Pharm. 18 (2021) 593–609, https://doi.org/10.1021/acs.molpharmaceut.0c00474.
[23] J. Qiao, M. Purro, Z. Liu, M.P. Xiong, Effects of polyethyelene glycol-desferrioxamine:gallium conjugates on *Pseudomonas aeruginosa* outer membrane permeability and vancomycin potentiation, Mol. Pharm. 18 (2021) 735–742, https://doi.org/10.1021/acs.molpharmaceut.0c00820.
[24] J. Qiao, Z. Liu, S. Cui, T. Nagy, M.P. Xiong, Synthesis and evaluation of an amphiphilic deferoxamine:gallium-conjugated cationic random copolymer against a murine wound healing infection model of *Pseudomonas aeruginosa*, Acta Biomater. 126 (2021) 384–393, https://doi.org/10.1016/j.actbio.2021.03.005.
[25] Z. Liu, T. Huang, Q. Shi, Z. Deng, S. Lin, Catechol siderophores framed on 2,3-dihydroxybenzoyl-L-serine from *Streptomyces varsoviensis*, Front. Microbiol. 14 (2023), https://doi.org/10.3389/fmicb.2023.1182449.
[26] M. Liu, X. Wu, J. Li, L. Liu, R. Zhang, D. Shao, X. Du, The specific anti-biofilm effect of gallic acid on *Staphylococcus aureus* by regulating the expression of the *ica* operon, Food Control 73 (2017) 613–618, https://doi.org/10.1016/j.foodcont.2016.09.015.
[27] Y. Liu, J. Chen, H. Li, Y. Wang, Nanocomplexes film composed of gallic acid loaded ovalbumin/chitosan nanoparticles and pectin with excellent antibacterial activity: preparation, characterization and application in coating preservation of salmon fillets, Int. J. Biol. Macromol. 259 (2024) 128934, https://doi.org/10.1016/j.ijbiomac.2023.128934.
[28] M. Marzano, N. Borbone, F. Amato, G. Oliviero, P. Fucile, T. Russo, F. Sannino, M. Marzano, N. Borbone, F. Amato, G. Oliviero, P. Fucile, T. Russo, F. Sannino, 3D chitosan-gallic acid complexes: assessment of the chemical and biological properties, Gels 8 (2022), https://doi.org/10.3390/gels8020124.
[29] H. Khatoon, S.M.M. Faudzi, T. Sohajda, Mechanisms and therapeutic applications of β-cyclodextrin in drug solubilisation and delivery systems, Chem. Biodivers. 22 (2025) e00359, https://doi.org/10.1002/cbdv.202500359.
[30] G. Hoti, N. Bajwa, F. Caldera, P.A. Singh, I. Hussein, C. Cecone, A. Matencio, R. Spagnolo, M. Argenziano, R. Cavalli, J. Madan, F. Trotta, Cyclodextrin-based therapeutics delivery systems: a review of current clinical trials, Curr. Res. Pharmacol. Drug Discov. 9 (2025) 100232, https://doi.org/10.1016/j.crphar.2025.100232.
[31] J. Szejtli, Introduction and general overview of cyclodextrin chemistry, Chem. Rev. 98 (1998) 1743–1754, https://doi.org/10.1021/cr970022c.
[32] W. Xu, X. Li, L. Wang, S. Li, S. Chu, J. Wang, Y. Li, J. Hou, Q. Luo, J. Liu, Design of cyclodextrin-based functional systems for biomedical applications, Front. Chem. 9 (2021), https://doi.org/10.3389/fchem.2021.635507 (accessed October 1, 2023).
[33] Á. Sarabia-Vallejo, M. del M. Caja, A.I. Olives, M.A. Martín, J.C. Menéndez, Cyclodextrin inclusion complexes for improved drug bioavailability and activity: synthetic and analytical aspects, Pharmaceutics 15 (2023) 2345, https://doi.org/10.3390/pharmaceutics15092345.
[34] D. Boczar, K. Michalska, Cyclodextrin inclusion complexes with antibiotics and antibacterial agents as drug-delivery systems—a pharmaceutical perspective, Pharmaceutics 14 (2022) 1389, https://doi.org/10.3390/pharmaceutics14071389.
[35] T.E. Clarke, V. Braun, G. Winkelmann, L.W. Tari, H.J. Vogel, X-ray crystallographic structures of the *Escherichia coli* periplasmic protein FhuD bound to hydroxamate-type siderophores and the antibiotic albomycin*, J. Biol. Chem. 277 (2002) 13966–13972, https://doi.org/10.1074/jbc.M109385200.
[36] A.J. Arifin, M. Hannauer, I. Welch, D.E. Heinrichs, Deferoxamine mesylate enhances virulence of community-associated methicillin resistant *Staphylococcus aureus*, Microbes Infect. 16 (2014) 967–972, https://doi.org/10.1016/j.micinf.2014.09.003.
[37] R.S. Patel, M. Parmar, Doxycycline Hyclate, in: StatPearls, StatPearls Publishing, Treasure Island (FL), 2024. http://www.ncbi.nlm.nih.gov/books/NBK555888/ (accessed December 11, 2024).
[38] A.C. Kogawa, A. Zoppi, M.A. Quevedo, H.R. Nunes Salgado, M.R. Longhi, Increasing doxycycline hyclate photostability by complexation with β-cyclodextrin, AAPS PharmSciTech 15 (2014) 1209–1217, https://doi.org/10.1208/s12249-014-0150-7.
[39] M. Pandey, P. Rani, L. Adhikari, M. Gupta, A. Semalty, M. Semalty, Preparation and characterization of cyclodextrin complexes of doxycycline hyclate for improved photostability in aqueous solution, J. Incl. Phenom. Macrocycl. Chem. 102 (2022) 271–278, https://doi.org/10.1007/s10847-021-01116-z.
[40] J. Shwetha, K. Pruthviraj, T.B. Rao, A.K. Solomon, Assessing the structural, antibacterial, and dissolution properties of 1:1 doxycycline/β-cyclodextrin complexes, J. Mol. Struct. 1321 (2025) 139977, https://doi.org/10.1016/j.molstruc.2024.139977.
[41] M100-Ed36, Performance Standards for Antimicrobial Susceptibility Testing, 36th Edition, Clinical & Laboratory Standards Institute (CLSI), 2025. https://clsi.org/standards/products/microbiology/documents.
[42] B.L.M. DeJonge, C. Slover, S.T. Nguyen, C. Longshaw, M. Takemura, N. Anan, H. Yamashiro, Y. Yamano, The impact of commercially available media on cefiderocol susceptibility testing by broth microdilution method, J. Clin. Microbiol. 63 (2025) e0047125, https://doi.org/10.1128/jcm.00471-25.
[43] J.S.L. Ii, A.J. Mathers, A.M. Bobenchik, A.L. Bryson, S. Campeau, S.K. Cullen, T. Dingle, G. Esparza, R.M. Humphries, T.J. Kirn, J. Lutgring, N. Narayanan, E. Palavecino, V.M. Pierce, A.N. Schuetz, S. Sharp, P.J. Simner, P.D. Tamma, M. P. Weinstein, Performance Standards for Antimicrobial Susceptibility Testing 35, 2025. https://clsi.org/shop/standards/m100/.
[44] M. Birus, M. Gabricevic, O. Kronja, B. Klaic, 13C and 1H NMR line broadening in desferrioxamine B spectra. Kinetics and mechanism of siderophore chemistry, Inorg. Chem. 34 (1995) 3110–3113, https://doi.org/10.1021/ic00115a047.
[45] G. Vecchio, T. Campagna, R. Marchelli, E. Rizzarelli, Synthesis and conformation of β-cyclodextrin functionalised with a phenylalanine derivative. Conformational changes induced by metal ions, J. Supramol. Chem. 1 (2001) 117–124, https://doi.org/10.1016/S1472-7862(01)00017-X.
[46] V. Cucinotta, F. D'Alessandro, G. Impellizzeri, G. Pappalardo, E. Rizzarelli, G. Vecchio, Cyclopeptide functionalized β-cyclodextrin. A new class of potentially enzyme mimicking compounds with two recognition sites, J. Chem. Soc. Chem. Commun. (1991) 293–294, https://doi.org/10.1039/C39910000293.
[47] L. Lambs, B. Decock-Le Reverend, H. Kozlowski, G. Berthon, Metal ion-tetracycline interactions in biological fluids. 9. Circular dichroism spectra of calcium and magnesium complexes with tetracycline, oxytetracycline, doxycycline, and chlortetracycline and discussion of their binding modes, Inorg. Chem. 27 (1988) 3001–3012, https://doi.org/10.1021/ic00290a022.
[48] L.J. Hughes, J.J. Stezowski, R.E. Hughes, Chemical-structural properties of tetracycline derivatives. 7. Evidence for the coexistence of the zwitterionic and nonionized forms of the free base in solution, J. Am. Chem. Soc. 101 (1979) 7655–7657, https://doi.org/10.1021/ja00520a003.
[49] E. Farkas, É.A. Enyedy, H. Csóka, A comparison between the chelating properties of some dihydroxamic acids, desferrioxamine B and acetohydroxamic acid, Polyhedron 18 (1999) 2391–2398, https://doi.org/10.1016/S0277-5387(99)00144-8.
[50] B. Monzyk, A.L. Crumbliss, Kinetics and mechanism of the stepwise dissociation of iron(III) from ferrioxamine B in aqueous acid, J. Am. Chem. Soc. 104 (1982) 4921–4929, https://doi.org/10.1021/ja00382a031.
[51] M.S. Masoud, A.E. Ali, S.S. Haggag, N.M. Nasr, Spectroscopic studies on gallic acid and its azo derivatives and their iron(III) complexes, Spectrochim. Acta A Mol. Biomol. Spectrosc. 120 (2014) 505–511, https://doi.org/10.1016/j.saa.2013.10.054.
[52] A.E. Fazary, M. Taha, Y.-H. Ju, Iron complexation studies of gallic acid, J. Chem. Eng. Data 54 (2009) 35–42, https://doi.org/10.1021/je800441u.
[53] H.K.J. Powell, M.C. Taylor, Interactions of iron(II) and iron(III) with gallic acid and its homologues: a potentiometric and spectrophotometric study, Aust. J. Chem. 35 (1982) 739–756, https://doi.org/10.1071/ch9820739.
[54] G. Hostnik, J. Tošović, S. Štumpf, A. Petek, U. Bren, The influence of pH on UV/Vis spectra of gallic and ellagic acid: a combined experimental and computational study, Spectrochim. Acta A Mol. Biomol. Spectrosc. 267 (2022) 120472, https://doi.org/10.1016/j.saa.2021.120472.
[55] P.V. Cherepanov, Md.A. Rahim, N. Bertleff-Zieschang, Md.A. Sayeed, A. P. O'Mullane, S.E. Moulton, F. Caruso, Electrochemical behavior and redox-dependent disassembly of gallic acid/FeIII metal–phenolic networks, ACS Appl. Mater. Interfaces 10 (2018) 5828–5834, https://doi.org/10.1021/acsami.7b19322.
[56] J.W. Southwell, C.M. Black, A.-K. Duhme-Klair, Experimental methods for evaluating the bacterial uptake of trojan horse antibacterials, ChemMedChem 16 (2021) 1063–1076, https://doi.org/10.1002/cmdc.202000806.
[57] K.N. Raymond, B.E. Allred, A.K. Sia, Coordination chemistry of microbial iron transport, Acc. Chem. Res. 48 (2015) 2496–2505, https://doi.org/10.1021/acs.accounts.5b00301.
[58] H. Killmann, C. Herrmann, A. Torun, G. Jung, V. Braun, TonB of *Escherichia coli* activates FhuA through interaction with the beta-barrel, Microbiology (Reading) 148 (2002) 3497–3509, https://doi.org/10.1099/00221287-148-11-3497.
[59] N. Noinaj, M. Guillier, T.J. Barnard, S.K. Buchanan, TonB-dependent transporters: regulation, structure, and function, Ann. Rev. Microbiol. 64 (2010) 43–60, https://doi.org/10.1146/annurev.micro.112408.134247.